

## WIND-DISK SHOCKS AROUND T TAURI STARS

L. HARTMANN<sup>1</sup> AND J. C. RAYMOND

Harvard-Smithsonian Center for Astrophysics

Received 1988 May 2; accepted 1988 July 27

## ABSTRACT

We suggest that the winds of T Tauri stars are heated at distances of 50–100 AU by oblique shocks with circumstellar disks, producing the observed high-velocity forbidden-line emission. The low shock velocities characteristic of this model provide low-excitation emission and line profiles in reasonable agreement with observations. The blueshifted character of the observed emission is explained by a combination of disk occultation of the receding flow, plus a modest collimation of the observable wind by the disk envelope. Instabilities at the wind-disk interface may be important in producing the observed emission. We suggest further observational tests of this picture.

*Subject headings:* shock waves — stars: circumstellar shells — stars: pre-main-sequence — stars: winds

## I. INTRODUCTION

High-velocity, broad [O I] and [S II] emission lines are observed in some T Tauri stars (TTs). The forbidden emission is thought to be formed in the distant, asymptotically expanding regions of stellar winds (Jankovics, Appenzeller, and Krautter 1983, hereafter JAK; Appenzeller, Jankovics, and Ostriker 1984, hereafter AJO; Edwards *et al.* 1987). In principle, this emission can be used to investigate the outflow geometry interior to the jets and Herbig-Haro (HH) objects driven by some TTs (e.g., Mundt 1985), helping to show whether the mass loss is collimated close to the star (e.g., Pudritz and Norman 1983) or whether large-scale collimation by the interstellar medium is required (cf. Cantó 1980; Barral and Cantó 1981; Königl 1982; Cantó, Tenorio-Tagle, and Rozyczka 1988).

The [O I] and [S II] emission may also provide a useful tool for determining the sizes of circumstellar disks around TTs. The forbidden-line emission is nearly always blueshifted with respect to the star. This result is attributed to occultation of the optically thin lines by circumstellar disks which extend out to 50–100 AU (JAK; AJO; Edwards *et al.* 1987).

The most puzzling aspect of the forbidden-line emission is the mechanism responsible for heating the wind. The wind density falls below the critical densities for collisional de-excitation of the forbidden lines at distances of thousands of stellar radii. This far from the central star, one would have expected radiative cooling and adiabatic expansion to cool the gas well below the temperatures required to excite the observed lines. We suggest that the [O I] and [S II] emission is the observational signature of shock heating of a stellar wind as it strikes the circumstellar disk obliquely. Our model naturally explains the heating of the stellar wind at large radial distances required by observations.

The wind-disk shock picture has several important ramifications. It suggests that despite the evidence for bipolar flows and jets, T Tauri stars have a significant component of their mass loss in the near-equatorial region. This picture also

implies that the forbidden-line profiles depend upon a combination of disk geometry and outflow characteristics.

We discuss the difficulty of producing forbidden emission in a cooling stellar wind in § II. In § III we discuss the physical conditions required to produce adequate emission from a wind-disk shock. A simple theory for oblique shocks is presented in § IV, and detailed calculations of forbidden-line fluxes and line profiles are presented in § V. We summarize our results in § VI.

## II. STELLAR WIND MODELS

a) *Observational Constraints*

Roughly a fifth of all T Tauri stars exhibit optical [O I] emission with equivalent widths  $\geq 1 \text{ \AA}$  (Strom *et al.* 1988). When studied at high spectral resolution, these lines generally exhibit velocity widths comparable to the stellar surface escape speed (150–200 km s<sup>-1</sup>; Fig. 1), strongly suggesting that the forbidden-line emission originates in a stellar wind (JAK; AJO; Edwards *et al.* 1987). Many objects also show [S II]  $\lambda\lambda 6717, 6731$  emission (though not all; it is not apparent in DF Tau). Because the [O I] and [S II] lines are collisionally quenched at modest densities, the observed high-velocity emission is probably formed in low-density wind far from the central star. Spectroscopic observations usually use slits of  $\sim 1''\text{--}2''$  centered on the star, so the emitting regions are generally  $\lesssim 160 \text{ AU}$  in radius for stars in Taurus-Auriga.

The forbidden-line emission is nearly always blueshifted from the stellar rest velocity (cf. Fig. 1), requiring occultation of the receding flow at large distances. JAK, AJO, and Edwards *et al.* (1987) argue that this occultation is caused by a circumstellar disk. The case for circumstellar disks is strengthened by the presence of excess infrared emission from the forbidden-line T Tauri stars, which is most plausibly interpreted as dust radiation from disks (Adams, Lada, and Shu 1987; Kenyon and Hartmann 1987).

The observed [O I] luminosities range from about  $10^{29}$  to  $10^{30}$  ergs s<sup>-1</sup>. The [S II]  $\lambda 6731/\lambda 6717$  ratio is generally greater than 1.6, suggesting electron densities near the critical value of  $\sim 10^4 \text{ cm}^{-3}$ . Combining the density with the observed line luminosity, and assuming an excitation temperature of  $10^4 \text{ K}$ , one can find the emitting volume and thus a characteristic

<sup>1</sup> Visiting Astronomer, Kitt Peak National Observatory, National Optical Astronomy Observatories, which is operated by Associated Universities for Research in Astronomy, Inc., under contract with the National Science Foundation.

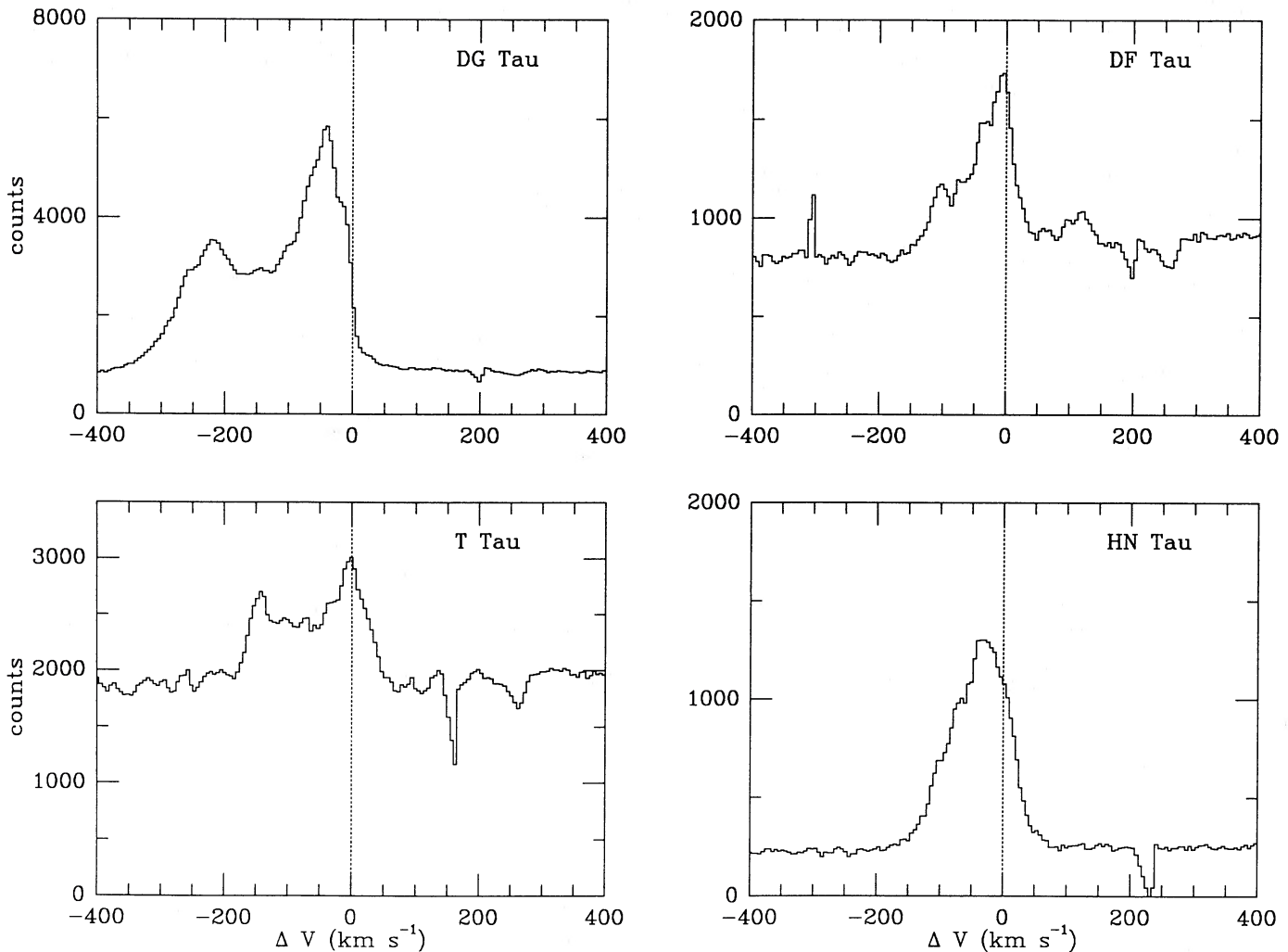


FIG. 1.—[O I]  $\lambda 7774$  line profiles of DG Tau, DF Tau, T Tau, and HN Tau, taken at Kitt Peak with the 4 m telescope and TI CCD in 1988 January. Velocity resolution is about  $12 \text{ km s}^{-1}$ . The dashed line indicates the rest velocity of [O I] in the stellar rest frame. The typical blueshifted, broad emission seen in some T Tauri stars is present, similar to that observed by AJO and Edwards *et al.* (1987). No attempt has been made to correct for night-sky emission, which could contribute some narrow (essentially unresolved) emission near the low-velocity peaks of DG, DF, and T Tau. A more detailed analysis of these data will be presented later.

radius ( $\sim 50 \text{ AU}$ ; JAK; AJO; Edwards *et al.* 1987). Using the observed line shifts of  $100\text{--}200 \text{ km s}^{-1}$ , Edwards *et al.* find mass-loss rates  $\dot{M} \sim 10^{-8}$  to  $10^{-7} M_{\odot} \text{ yr}^{-1}$ , in reasonable agreement with other estimates (cf. Hartmann 1986).

Both AJO and Edwards *et al.* (1987) conclude that a simple flat disk occultation of a spherically symmetric flow cannot completely account for the observed blueshifted emission. If the flow diverges too rapidly, one should occasionally see substantially redshifted emission when the disk axis is appreciably inclined to the line of sight. Hence, AJO and Edwards *et al.* suggest that the outflows are somewhat “bipolar” or conical (i.e., restricted to angles less than  $90^{\circ}$  from the disk axis). However, the required collimation is modest; Edwards *et al.* suggest that the maximum angle from the disk axis allowed by the observations is  $\sim 70^{\circ}$ . The double-peaked profiles sometimes observed (Fig. 1) suggest that some flows may be more like hollow cones (AJO; Edwards *et al.* 1987).

#### b) Wind Models

The inner wind regions of T Tauri stars must be heated to temperatures  $\sim 10^4 \text{ K}$  in order to explain Balmer line emission

(Kuhi 1964; Kuan 1975; DeCampli 1981; Hartmann, Edwards, and Avrett 1982; Hartmann 1986). However, the densities required to produce the Balmer lines are so large that [O I] and [S II] emission is strongly quenched. AJO and Edwards *et al.* (1987) presume that the forbidden-line emission naturally arises in the outer, low-density wind. The question is whether the stellar wind can maintain sufficiently high gas temperatures to excite this emission in the face of adiabatic expansion and radiative cooling.

To investigate this problem, we computed spherically expanding wind models with adiabatic and radiative cooling. The assumption of radial expansion is suggested by the large velocity widths of the observed emission lines, which indicate expansion in the line of sight comparable to the likely stellar wind terminal velocities (see Edwards *et al.* 1987 for a more detailed discussion of possible flow geometries). No large-scale heating was included other than absorption of X-rays from coronal gas at the base of the wind.

The model calculations follow an element of gas as it cools and recombines, typically for 200 time steps. The computation ends when the gas temperature falls below  $1000 \text{ K}$ , since the

lines of interest are not effectively excited at lower temperatures. The cooling, ionization evolution, and emission spectrum are computed by codes developed for interstellar shock waves, with current atomic rates summarized in Cox and Raymond (1985) and some modifications for high densities discussed in Mauche and Raymond (1987). Of particular importance for the T Tauri wind models are low-temperature dielectronic recombination (Nussbaumer and Storey 1983), charge transfer (Butler and Dalgarno 1980), and Auger ionization by X-ray photoionization of the K shells of carbon, nitrogen, and oxygen. Probably the most serious problem with the models is the lack of a detailed treatment of the hydrogen level populations. Since we care mostly about regions where the electron density is low enough for effective excitation of [O I] ( $\lesssim 10^6 \text{ cm}^{-3}$ ) and since the Sobolev optical depths for Ly $\alpha$  are only on the order of 1000, this should not be too serious. Intense chromospheric Ly $\alpha$  radiation may be present, however, affecting the ionization state and effective cooling rate of hydrogen.

Models were computed with mass loss rates of  $10^{-9}$ ,  $10^{-8}$ , and  $10^{-7} M_{\odot} \text{ yr}^{-1}$ . The initial radius was  $3 \times 10^{11} \text{ cm}$  for our basic wind models. We adopted an initial temperature of  $2 \times 10^6 \text{ K}$ , a typical value for a corona around a late-type star, and the expansion velocity was assumed to be constant at  $200 \text{ km s}^{-1}$ . No further energy was added to the expanding gas, except that EUV and X-ray emission produced in the high-temperature region ionizes and heats the cool gas farther out. To simulate situations in which the wind begins to cool from somewhat lower temperatures, and is ionized by a thin underlying X-ray-emitting corona, we also ran models with the ionizing fluxes reduced by factors of 10 and 100. The Allen (1973) "cosmic" abundance set is used throughout.

The predicted luminosities of the strong optical emission lines are given in Table 1. The mass-loss rate is given in solar masses per year, and the X-ray luminosity is the *Einstein* Imaging Proportional Counter band luminosity of the cooling gas with the reduction by a factor of 1, 10, or 100 as discussed above. This is *not* the X-ray luminosity which the *Einstein* satellite would have observed, however, since most of the

X-rays are absorbed in the wind. In the  $10^{-8} M_{\odot} \text{ yr}^{-1}$ ,  $9.1 \times 10^{30} \text{ ergs s}^{-1}$  model, for example, the X-rays are attenuated by a factor of 1000 by the time the calculation terminates. We do not tabulate attenuated X-ray fluxes because the attenuation does not cease when we cut off the computation at 1000 K. It is also possible that, while [O I] cannot be collisionally excited below 1000 K, there may be some further H $\beta$  emission by recombination at lower temperatures.

Figure 2 shows the time evolution of the temperature and cooling rate for an element of gas in the  $10^{-8} M_{\odot} \text{ yr}^{-1}$  model with the X-ray fluxes reduced by a factor of 10. Photoelectric heating is negligible until the gas begins to recombine at a time of  $10^3 \text{ s}$ . The heating rises steeply until it balances radiative cooling in the plateau region between  $1 \times 10^3$  and  $2 \times 10^3 \text{ s}$ . Beyond that time the radiative cooling drops and adiabatic expansion cooling dominates. The apparent rise in adiabatic cooling at large times reflects a decrease in  $N_e$ ; the adiabatic cooling rate per cubic centimeter actually decreases with time.

Two trends in the emission as a function of mass-loss rate are apparent in Table 1. The low  $\dot{M}$  winds predict only weak [O I] emission, both because the quantity of cooling gas is relatively small and because adiabatic expansion cools the gas more effectively than radiative cooling in the temperature regime where [O I] could be formed. In the  $10^{-9} M_{\odot} \text{ yr}^{-1}$  model with high X-ray luminosity, the adiabatic cooling is so extreme that the gas falls below 1000 K while it is still fully ionized, resulting in a large [O III]/[O I] ratio. Aside from this ionization aspect, one sees as expected that the [O I] luminosity increases with X-ray luminosity. The higher  $\dot{M}$  winds produce [O I] luminosities in the observed range, but the high electron densities associated with high  $\dot{M}$  suppress [S II] quite strongly relative to [O I], so these models do not account for the observed emission lines either.

The wind models fail to reproduce the observations because radiative losses and adiabatic expansion cool the wind to temperatures below 1000 K at radii  $\lesssim 0.2 \text{ AU}$  (Fig. 2). At these distances wind densities are very large, resulting in unacceptable collisional de-excitation of [S II]. It is conceivable that the wind does not expand spherically, so that adiabatic cooling is less important. However, in that case the gas density does not fall off as  $r^{-2}$ , so that it is even more difficult to reach low enough densities to produce strong [S II]. Furthermore, the observations indicate a large line-of-sight velocity dispersion, which would be difficult to obtain without appreciable divergence in the flow.

In the absence of any heating other than coronal X-rays, the basic wind models in Table 1 cool rapidly by radiation. For example, the wind model in Figure 2 cools to 6000 K in a distance  $\sim 2 \times 10^{11} \text{ cm} \sim 1 R_{*}$ . In principle, magnetic wave modes might propagate through the wind, heating it to much larger distances (e.g., Hartmann, Edwards, and Avrett 1982). To investigate the effects of extended wave heating, we computed two other wind models for  $\dot{M} = 10^{-7} M_{\odot} \text{ yr}^{-1}$ , in which the calculation was started arbitrarily at some large distance and allowed to cool without further heating. One model was started at  $T_0 = 1 \times 10^4 \text{ K}$  at  $r_0 = 1 \times 10^{12} \text{ cm} \sim 3 R_{*}$ . This model produces adequate [O I], but far too little [S II]. Extending the wind heating to produce temperatures  $\gtrsim 10^4 \text{ K}$  at much larger distances is not feasible, because too much Balmer line and Mg II *h* and *k* emission is produced (Natta, Giovanardi, and Palla 1988; Calvet and Hartmann 1988). To try to avoid these problems, we computed another model starting at  $3 \times 10^{13} \text{ cm} = 2 \text{ AU}$ ,  $T = 5000 \text{ K}$ , and with

TABLE 1

LINE LUMINOSITIES FOR T TAURI WIND MODELS

log $\dot{M}$	RF <sup>a</sup>	log $L_x$	log $L_{H\beta}$	log $L_{[O I]}$	log $L_{[S II]}$	log $L_{[O III]}$
Basic Models: $T_0 = 2 \times 10^6 \text{ K}$ , $r_0 = 3 \times 10^{11} \text{ cm}$						
-9.....	1.0	30.61	28.53	24.72	23.49	28.78
-8.....	1.0	31.96	30.23	27.51	25.18	28.15
-7.....	1.0	33.00	31.28	26.88	21.53	27.99
-9.....	0.1	30.61	28.28	26.74	24.43	27.08
-8.....	0.1	31.96	29.49	27.89	25.43	27.76
-7.....	0.1	33.00	30.76	29.40	26.94	26.71
-9.....	0.01	30.60	28.11	26.04	23.92	26.57
-8.....	0.01	31.96	29.18	26.82	24.36	26.11
-7.....	0.01	33.00	30.30	29.08	26.57	26.00
Model with $T_0 = 1 \times 10^4 \text{ K}$ , $r_0 = 10^{12} \text{ cm}$ ; Fully Ionized, No X-Rays						
-7.....	...	...	30.84	29.39	26.95	00.00
Model with $T_0 = 5 \times 10^3 \text{ K}$ , $r_0 = 3 \times 10^{13} \text{ cm}$ ; 10% Ionized, No X-Rays						
-7.....	...	...	29.01	28.27	26.28	00.00

NOTE.— $\dot{M}$  is in units of  $M_{\odot} \text{ yr}^{-1}$ ; luminosities are in units of  $\text{ergs s}^{-1}$ . [O I] =  $\lambda 6300 + \lambda 6363$ , [S II] =  $\lambda 6717 + \lambda 6731$ , [O III] =  $\lambda 4959 + \lambda 5007$ .

<sup>a</sup> Factor multiplying X-ray emission; see text.

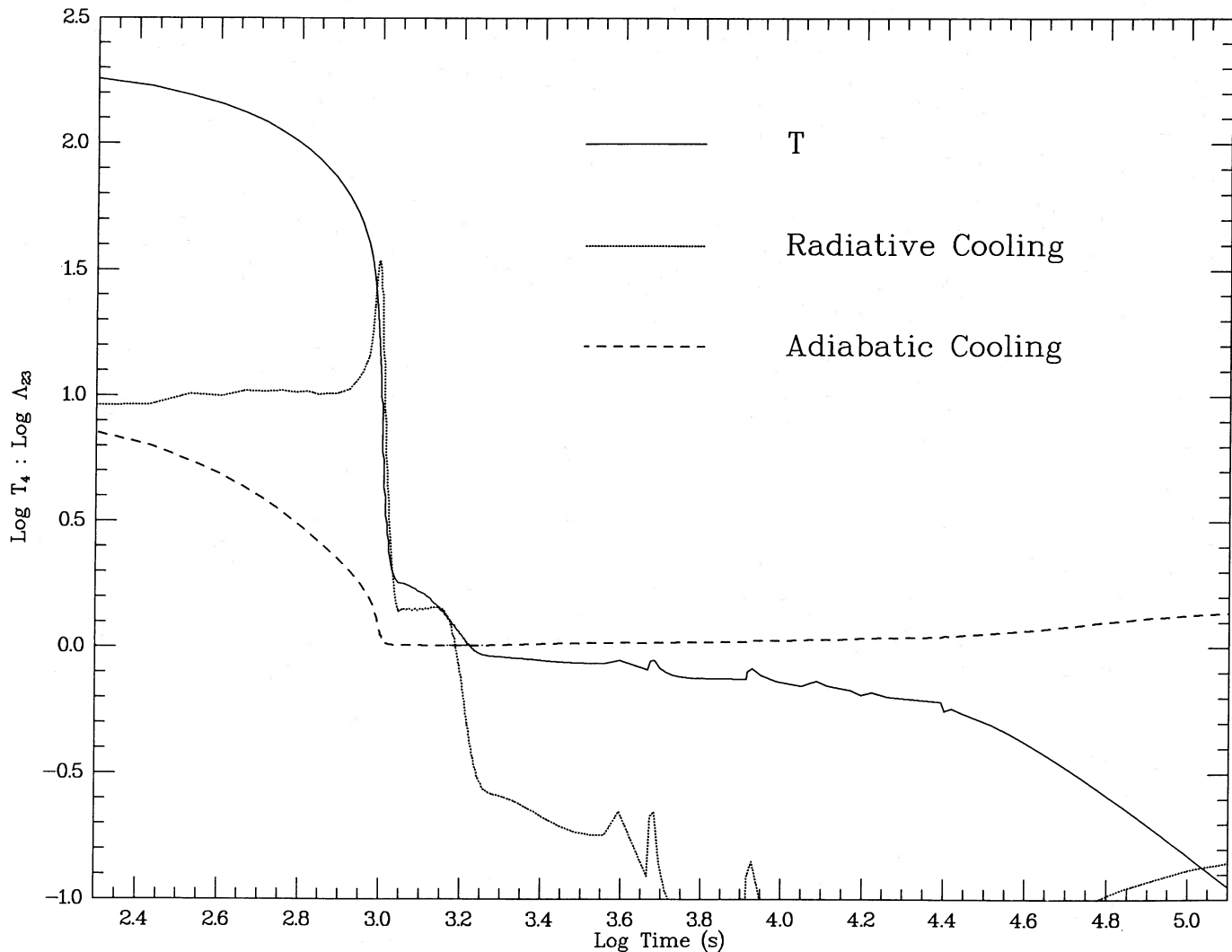


FIG. 2.—Time evolution of an expanding parcel of gas for the  $10^{-8} M_{\odot} \text{ yr}^{-1}$  model discussed in the text. The vertical axis is in units of  $\log(T/10^4 \text{ K})$  for the temperature (solid curve), while units of  $\log(10^{-23} \text{ ergs cm}^3)$  are used for the radiative and adiabatic cooling rates (dotted and dashed curves). The cooling coefficients must be multiplied by the product of electron and hydrogen densities  $N_e N_H$  to calculate the emission per cubic centimeter per second. The variation of quantities with radial distance in the wind can be found by simply multiplying the time by  $200 \text{ km s}^{-1}$ .

an initial hydrogen ionization fraction of 10%. Now the [O I] radiation is reduced, in part because adiabatic cooling dominates. Even at these relatively low densities the [S II] emission falls well below observations.

Table 2 presents a more complete list of the line emission for the  $10^{-8} M_{\odot} \text{ yr}^{-1}$  models, which is of general interest beyond the present narrow application to forbidden-line flows. The major feature of note is the large C IV flux predicted by the high X-ray luminosity model. The magnitude of the C IV emission is at the high end of observed fluxes (Cram, Giampapa, and Imhoff 1980; Brown, Ferraz, and Jordan 1984; Lago, Penston, and Johnstone 1985). This calculation does not take into account the absorption of X-rays by the stellar photosphere. In particular, the He II flux might be increased somewhat by accounting for emission from stellar layers.

We also call attention to the [O III] fluxes for the large X-ray luminosity models. Upper limits for [O III] are not generally available in the literature; we suspect that the  $RF = 1$  models might be ruled out by careful observations.

### c) Wind-heating Mechanisms

Our results indicate that T Tauri winds must be heated at large distances from the star to produce the observed [S II] emission. It is difficult to attribute this heating to a stellar source of energy. The models show that photoionization by coronal X-rays does not agree with observations. Magnetic wave modes can in principle carry energy out to large distances from the star, but such heating is hard to understand because the forbidden-line regions seem to be far beyond the wind Alfvén radius. This follows from the Weber-Davis spin-down time scale,

$$\tau_J = \frac{3k}{2} \frac{M}{\dot{M}} \left( \frac{R_*}{R_A} \right)^2 \quad (1)$$

(Belcher and MacGregor 1976). In this equation  $k$  is the moment-of-inertia constant,  $\sim 0.2$  for a fully convective star. If  $R_A/R_*$  is much larger than  $\sim 10^2$ , for  $\dot{M} \gtrsim 10^{-8} M_{\odot} \text{ yr}^{-1}$  the spin-down time would become very much shorter than a

TABLE 2  
EMISSION-LINE LUMINOSITIES FOR  $10^{-8} M_{\odot} \text{ yr}^{-1}$  WINDS

ION	$\lambda$ (Å)	LUMINOSITY ( $10^{29}$ ergs $\text{s}^{-1}$ )		
		RF = 1.0	RF = 0.10	RF = 0.01
He I	5876	0.78	0.031	0.14
He II	1640	56	3.4	1.9
C II	1335	28	4.4	2.6
C III]	1909	146	5.5	1.7
C IV	1550	760	63	60
N V	1240	42	31	31
O III]	1664	54	5.3	3.4
O IV]	1400	91	9.7	8.1
Mg II	2800	106	28	5.6
Si IV	1400	120	3.8	3.6
Ca II	3945	28	4.3	2.0
Fe II	2600	24	7.6	1.5

typical T Tauri star age of  $\geq 10^5$  yr. In addition, such a large Alfvén radius would impart a very large azimuthal velocity to the wind for typical T Tauri rotational velocities of 10–20  $\text{km s}^{-1}$  (Bouvier *et al.* 1986; Hartmann *et al.* 1986), producing asymptotic wind acceleration beyond 200  $\text{km s}^{-1}$  (see Belcher and MacGregor 1976). Therefore, the forbidden-line emitting gas must be in a region where the poloidal magnetic energy density is far less than the wind energy density. It is not clear why magnetic wave modes should play such an important role in heating under these circumstances. Moreover, the mechanism damping the waves at the appropriate radial distances is not apparent. Because of these problems it seems more likely that the required wind heating at large distances is caused by some external agent.

### III. SHOCK WAVE MODELS

#### a) Basic Considerations

In principle, shock waves might produce the distant wind heating required by the observed forbidden-line emission. Shock models have been successfully applied to HH objects, which often have strong [O I] and [S II] emission (see Schwartz 1983). Bow-shock models for HH objects can produce line profiles that are broad and double-peaked, with a peak at zero velocity (Hartigan, Raymond, and Hartmann 1987), just as observed in TTs (AJO; Edwards *et al.* 1987; Fig. 1). However, the bow-shock models predict that the line width is essentially equal to the maximum shock velocity (Hartigan, Raymond, and Hartmann 1987). In the case of TTs, the [O I] line widths are typically  $\geq 150 \text{ km s}^{-1}$ . A shock velocity of this magnitude would result in strong [O III] emission and other high-excitation lines (Hartigan, Raymond, and Hartmann 1987), which are not observed (Edwards 1988). Thus it is difficult to see how the observed emission can be explained by an HH object model.

To investigate what types of shocks are needed to explain the observations, we have computed a series of steady plane-parallel shock models using the code described by Cox and Raymond (1985). We have assumed solar abundances and a preshock ionization fraction  $f$  of 0.01 in these models. The effects of changing  $f$  are discussed below.

We assume that the flow entering the shock is atomic rather than molecular (see Rawlings, Williams, and Cantó 1988). If this were not the case, then slow shocks could not dissociate  $\text{H}_2$ , and molecular cooling would greatly reduce the [O I] emission (e.g., Chernoff, Hollenbach, and McKee 1982; Draine,

Roberge, and Dalgarno 1983). However, the photospheric radiation field should destroy  $\text{H}^-$  sufficiently to prevent substantial  $\text{H}_2$  formation via  $\text{H}^- + \text{H} \rightarrow \text{H}_2 + e$ . Molecules may also form as the shocked gas cools past  $\sim 3000 \text{ K}$  (Neufeld 1987), but this can be prevented by the stellar radiation field. Mass loading of the wind with dust and molecular material from the interstellar medium may eventually occur (Rawlings, Williams, and Cantó 1988).

The line emission predicted by the plane-parallel shock models is given in Table 3. The available observations indicate that  $[\text{N II}] \lambda 6583 < 0.07 [\text{O I}]$  for all but a few objects. In the sample of Edwards *et al.* (1987), the ratio of  $[\text{S II}] (\lambda 6731 + \lambda 6717)/[\text{O I}]$  ranges from 0.1 to 0.5. Applying these models to the observational constraints, we find the permitted values of shock velocity and preshock density indicated in Figure 3. The (usual) upper limits on [N II] and the strengths of [S II] relative to [O I] combine to limit the shock velocities to  $\lesssim 40 \text{ km s}^{-1}$ . This is very much lower than the wind velocities  $\sim 200 \text{ km s}^{-1}$ , and thus any shock driven by the wind producing the forbidden emission *must be oblique*.

This upper limit on the shock velocity is not very sensitive to the preshock ionization fraction. The 40  $\text{km s}^{-1}$  shocks ionize the gas to  $f \sim 8\%$ . The ionization states of oxygen and nitrogen are similar to that of hydrogen, so a preshock ionization fraction  $f$  implies similar fractions of  $\text{O}^+$  and  $\text{N}^+$  in the shocked gas. Thus large  $f$  will reduce the [O I] and [N I] luminosities and increase the [O II] and [N II] intensities. The observational upper limit  $[\text{N II}]/[\text{O I}] < 0.07$  translates into an approximate condition  $f \lesssim 15\%$ .

#### b) Wind-Disk Shocks

Jets can have internal oblique shocks (e.g., Mundt 1985), in principle explaining the observed emission. However, as dis-

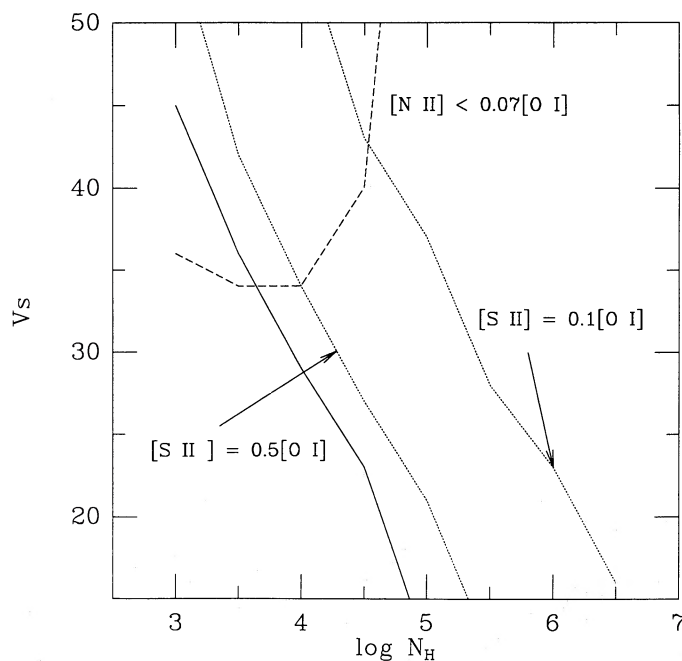


FIG. 3.—Application of observational constraints to the results from the shock models listed in Table 3. Models with  $[\text{N II}] < 0.07[\text{O I}]$  lie to the right of and below the dashed line. Models with  $\lambda 6731 > 1.6 \lambda 6717$  lie to the right of the solid line. The observational constraints of small [N II] emission and  $0.1 \leq [\text{S II}]/[\text{O I}] \leq 0.5$  constrain acceptable parameters to the area bounded by the dashed line and the two dotted lines.

TABLE 3  
SHOCK MODELS FOR  $f = 0.01$

V	F[O I]/N	I[O I]	I[O II]	I[N II]	I[6717]	I[6731]
N = 0.1000e+04						
15.	0.869e-07	100.0	0.2	0.7	66.1	46.7
20.	0.307e-06	100.0	2.7	0.6	58.3	42.3
30.	0.539e-06	100.0	6.5	2.4	50.3	44.5
40.	0.807e-06	100.0	19.1	16.4	33.5	46.7
50.	0.111e-05	100.0	34.7	44.1	20.6	38.1
N = 0.3160e+04						
15.	0.101e-06	100.0	1.7	0.6	62.9	48.2
20.	0.327e-06	100.0	2.5	0.6	54.4	44.3
30.	0.603e-06	100.0	5.6	2.3	38.5	46.3
40.	0.941e-06	100.0	12.6	14.2	18.7	35.1
50.	0.136e-05	100.0	16.9	33.6	9.3	20.1
N = 0.1000e+05						
15.	0.111e-06	100.0	1.5	0.6	55.1	50.8
20.	0.342e-06	100.0	2.3	0.6	45.3	46.5
30.	0.663e-06	100.0	4.2	2.2	24.4	40.3
40.	0.110e-05	100.0	6.3	11.4	8.7	18.8
50.	0.166e-05	100.0	6.4	21.2	3.9	8.8
N = 0.3160e+05						
15.	0.126e-06	100.0	2.3	0.6	41.4	52.1
20.	0.364e-06	100.0	1.9	0.6	31.9	45.3
30.	0.747e-06	100.0	2.5	1.9	12.7	25.8
40.	0.132e-05	100.0	2.5	7.4	3.7	8.4
50.	0.199e-05	100.0	2.1	10.3	1.7	3.8
N = 0.1000e+06						
15.	0.147e-06	100.0	0.9	0.6	26.3	44.7
20.	0.404e-06	100.0	1.2	0.5	18.4	34.4
30.	0.890e-06	100.0	1.1	1.4	5.8	12.9
40.	0.158e-05	100.0	0.8	3.7	1.6	3.8
50.	0.228e-05	100.0	0.7	4.0	1.0	2.3
N = 0.3160e+06						
15.	0.184e-06	100.0	0.5	0.5	14.1	28.9
20.	0.485e-06	100.0	0.6	0.4	8.9	19.1
30.	0.109e-05	100.0	0.4	0.8	2.5	5.8
40.	0.178e-05	100.0	0.3	1.4	1.0	2.2
50.	0.223e-05	100.0	0.4	1.6	0.8	1.8
N = 0.1000e+07						
15.	0.242e-06	100.0	0.2	0.4	6.9	15.0
20.	0.611e-06	100.0	0.2	0.3	3.9	8.8
30.	0.127e-05	100.0	0.1	0.4	1.2	2.8
40.	0.183e-05	100.0	0.1	0.6	0.7	1.6
50.	0.787e-06	100.0	0.1	0.6	0.6	1.4
N = 0.3160e+07						
15.	0.164e-06	100.0	0.1	0.2	3.3	7.5
20.	0.760e-06	100.0	0.1	0.2	1.8	4.0
30.	0.683e-06	100.0	0.0	0.2	0.7	1.7
40.	0.187e-05	100.0	0.0	0.2	0.5	1.2
50.	0.257e-05	100.0	0.0	0.2	0.4	1.0

NOTES.— $N$  is the preshock density in  $\text{cm}^{-3}$ ;  $V$  is the shock velocity in  $\text{km s}^{-1}$ ;  $F[\text{O I}]/N$  is the ratio of emergent flux in  $[\text{O I}]$  to the preshock density, where  $F$  is measured in  $\text{ergs cm}^2 \text{s}^{-1}$ . The intensities  $I$  are relative to  $[\text{O I}] = 100$ .  $[\text{O I}] = \lambda 6300 + \lambda 6363$ ,  $[\text{O II}] = \lambda 3727 + \lambda 3729$ ,  $[\text{N II}] = \lambda 6583 + \lambda 6548$ ,  $[\text{S II}] = \lambda 6717 + \lambda 6731$ ,  $[\text{C I}] = \lambda 9650$ .

cussed earlier, it is difficult to reconcile the idea of a collimated jet with the observed line widths comparable to the expected wind velocity. One would expect that some objects with collimated jets would have relatively narrow blueshifted emission; instead, the forbidden-emission line profiles generally extend from large negative velocities to near zero radial velocity.

The requirements of very oblique shocks and large line-of-sight velocity dispersions, along with the observed occultation of forbidden-line flows, suggests an interaction between the wind and a curved disk (Elmegreen 1978). Line widths will be large at most angles of observation, owing to the divergence of the impacting stellar wind around the disk. Because the disk surface becomes appreciably curved only at large distances (Kenyon and Hartmann 1987), the wind gets heated far from the star, as required by [S II] emission.

The component of the wind velocity normal to the disk surface is the shock velocity. In our models, which assume that the preshock wind has a very low temperature, the postshock velocity of the emitting gas is very small. Thus, the emitting gas will move essentially parallel to the disk surface, with a velocity given by conservation of the tangential velocity component.

Consider the disk very schematically as a tilted ring making an angle  $i$  with the equatorial plane. Very crudely, the "average" wind stream striking this ring flows at an angle  $\theta \sim i/2$  with respect to the disk midplane. If  $v$  is the wind velocity, the shock velocity is

$$v_s = v \sin(i - \theta) \sim \sin(i/2), \quad (2)$$

while the tangential velocity conserved across the shock is

$$v_T = v \cos(i - \theta) \sim \cos(i/2). \quad (3)$$

Edwards *et al.* (1987) concluded that the emission-line flow occurs in a slightly collimated cone, with  $i > 20^\circ$ . Setting  $i \sim 25^\circ$ , then  $v_s/v \sim 0.2$ . For a wind velocity of  $200 \text{ km s}^{-1}$ , the estimated shock velocity is  $\sim 40 \text{ km s}^{-1}$ , in the appropriate range to produce the observed emission-line ratios. The emitting material flows outward at about  $195 \text{ km s}^{-1}$  at an angle of  $25^\circ$  with respect to the midplane. With azimuthal symmetry this flow produces the required line widths at most angles of observation.

Inspection of Table 3 indicates that the [O I] emissivity for  $30\text{--}40 \text{ km s}^{-1}$  shocks is  $\sim 10^{-6} N \text{ ergs cm}^{-2} \text{ s}^{-1}$ , where  $N$  is the preshock density in  $\text{cm}^{-3}$ . The mass flux through the shock per unit area is  $N M_H v_s$ . Thus the minimum mass-loss rate required to produce the observed [O I] luminosity is

$$\dot{M}_{\min} = 2 \times 10^{-8} \left( \frac{L_{\text{OI}}}{3 \times 10^{29} \text{ ergs s}^{-1}} \right) M_\odot \text{ yr}^{-1}. \quad (4)$$

The mass-loss rate must be twice as large for a given luminosity if the occulting disk absorbs rather than reflects the [O I] emission. In addition, the total stellar mass-loss rate must be larger than  $\dot{M}_{\min}$ , since part of the wind does not strike the disk.

The total mass-loss rates implied by equation (4) are 2–3 times larger than those inferred by Edwards *et al.* (1987). The discrepancy probably arises because of the smaller efficiency of oblique shocks in exciting [O I] and because part of the wind misses the disk. Mass-loss rates of  $\sim 10^{-7} M_\odot \text{ yr}^{-1}$  required to produce the observed [O I] luminosities are at the high end of estimates for T Tauri stars (see e.g., Hartmann 1986). However, as pointed out by Strom *et al.* (1988) and Edwards *et al.* (1987), the [O I] sources tend to be more luminous than the average

TTSs, and so perhaps the higher mass-loss rates required are to be expected.

The observational constraints indicated in Figure 3 suggest that acceptable preshock wind densities are in the range  $10^4\text{--}10^5 \text{ cm}^{-3}$ . The required preshock densities might be larger at the lowest shock velocities, but these shocks are not very efficient in producing [O I] emission (Table 3) and so probably can be ignored. With  $\dot{M} \sim 10^{-7} M_\odot \text{ yr}^{-1}$ , these densities imply an emitting region  $\sim 30\text{--}100 \text{ AU}$  in radial extent, in agreement with the estimates of Edwards *et al.* (1987).

A useful feature of the model is that it makes a connection between the modest collimation inferred from observations and the (oblique) shock velocity. The disk must be there in any event in order to occult the receding flow. The biggest question is whether the disk can be sufficiently thick (or curved) to produce a large enough shock velocity. The vertical scale height of a rotating disk in hydrostatic equilibrium is  $H = (c_s^2 R^3 / GM)^{1/2}$ , where  $c_s$  is the sound speed,  $R$  is the radial distance in the disk plane, and  $M$  is the central mass. For a  $1 M_\odot$  star with a surface temperature of 4000 K, assuming that the disk temperature falls off as  $r^{-1/2}$ ,  $H \sim 16 \text{ AU}$  at  $R = 100 \text{ AU}$ . This would suggest that the wind-disk shock need be only 1–2 scale heights above the midplane. However, the detailed models developed in the following sections work less well, because the disk curvature is less than assumed here. Furthermore, optically thick disks probably have internal temperatures falling off more rapidly than  $r^{-1/2}$ , owing to the oblique streaming of the incident stellar radiation field (Adams and Shu 1986; Adams, Lada, and Shu 1987; Kenyon and Hartmann 1987).

#### IV. DETAILED MODEL FOR THE WIND-DISK SHOCK

We next construct a more quantitative model of a disk and of the interaction between the disk surface and the stellar wind. Cantó (1980), in considering the collision of a stellar wind with anisotropically distributed interstellar gas, suggested that the following regions will be present (Fig. 4): (1) the unshocked stellar wind; (2a) a flow region containing gas cooling down from passage through an oblique shock; (2b) a flow region in which the gas has cooled down and is joined by other previously shocked stellar wind material sliding along the surface of the external medium; and (3) undisturbed ambient medium. In this paper we make the simplifying assumptions that the emission we observe comes from the cooling region 2b, and that this cooling region is so thin that its shape is given essentially by the shock surface separating regions 1 and 2. We further assume that the radiating gas has cooled and compressed enough that its velocity perpendicular to the local shock surface is negligible, and thus its motion is entirely parallel to the shock surface at a speed given by momentum conservation across the shock (Cantó 1980).

We assume an isotropic, steady, radial, constant-velocity wind emanating from the central star, and assume that the disk has azimuthal symmetry. In a coordinate system where  $r$  is the radial distance from the central star to the shock surface and  $\theta$  is the angle measured from the disk midplane, the component of the wind velocity normal to the surface is the shock velocity,

$$v_s = vr / (r^2 + r'^2)^{1/2}, \quad (5)$$

while the wind velocity parallel to the surface is

$$v_T = vr' / (r^2 + r'^2)^{1/2}, \quad (6)$$

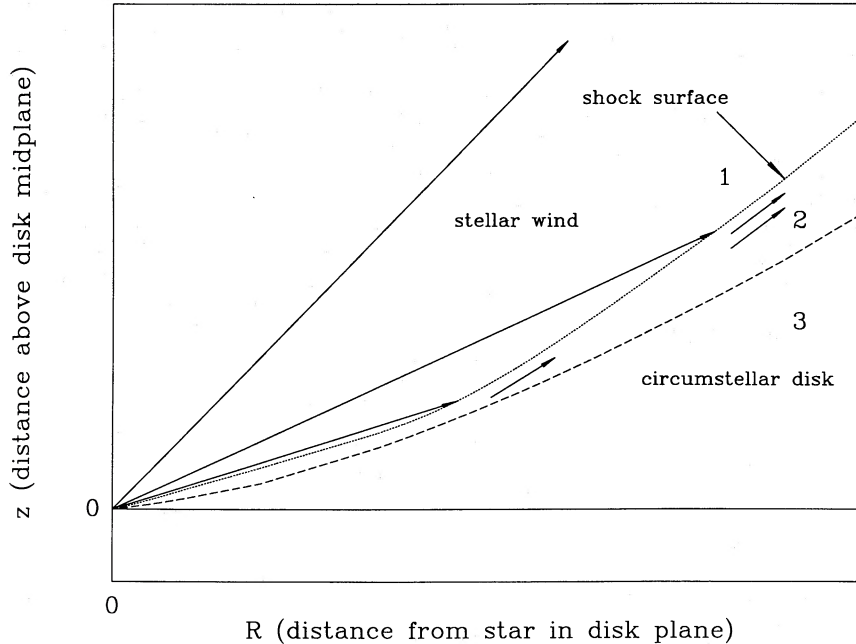


FIG. 4.—Structure assumed for the detailed wind-disk shock model, as described in the text

where  $r' = dr/d\theta$ . The simplest approximation to the shock surface is to balance the ram pressure of the wind against the pressure  $P(\text{ext})$  of the disk (Elmegreen 1978);

$$P(\text{ext}) = \rho_w v^2 \frac{r^2}{r^2 + r'^2}, \quad (7a)$$

where  $\rho_w$  is the wind density at  $r$ . This equation assumes that the wind material is stopped fairly quickly. On the other hand, Cantó (1980) assumes that post-shock gas material slides freely along the disk surface without further momentum loss. The equation of motion then becomes.

$$P(\text{ext}) = \rho_w v^2 \frac{r^2}{r^2 + r'^2} + \frac{r^2 + 2r'^2 - r'r}{(r^2 + r'^2)^{3/2}} \frac{W}{2\pi r \cos \theta}, \quad (7b)$$

where

$$W = \int_0^\theta \frac{1}{2} \dot{M}(\cos \theta) v_T d\theta$$

is the total accumulated momentum flux parallel to the shock surface. The second term on the right-hand side is the so-called centrifugal correction, accounting for the acceleration of flowing material as it travels along a curved surface (e.g., Hayes and Probst 1966). The integral  $W$  assumes that, in this steady state situation, a postshock laminar flow is set up, and that the momentum flow carried by the flowing material past  $\theta_i = \text{constant}$  includes all the momentum parallel to the shock surface accumulated between  $\theta = 0$  and  $\theta = \theta_i$ . Although Elmegreen's (1978) complete neglect of this effect seems extreme, the assumption of parallel momentum conservation is obviously an upper limit as well, since it seems likely that turbulent mixing between shocked wind and disk material (Elmegreen 1978; Kahn 1980) should result in some transfer of momentum to the disk. We will examine results in both limits.

The effect of the centrifugal term in equation (7b) is to flatten the shock surface and reduce its upward curvature. For cases of interest we find that the effect of including the centrifugal

correction is rather modest. The reason is that the shock surface is generally several scale heights above the midplane, where the disk density is varying very rapidly with height; thus modest changes in the ram pressure change the height of the pressure-balance surface by only a small amount.

The left-hand side of equation (7) denotes the external pressure distribution of the disk. The disk structure is more easily derived in a polar coordinate system  $(R, \phi, z)$ , where  $R$  is the distance measured in the disk midplane ( $z = 0$ ) and we assume azimuthal symmetry. In the  $R$ -direction the disk is assumed to be rotating in essentially Keplerian motion, while hydrostatic equilibrium is assumed in the  $z$ -direction (Shakura and Sunyaev 1973). The internal vertical temperature structure of the disk depends upon many parameters, such as the mass accretion rate (if any) and the detailed form of the viscosity, and on the absorption of light from the central star (Adams, Lada, and Shu 1987). The appropriate heating rates are poorly known, and so for simplicity we assume that the disk is vertically isothermal with some characteristic temperature  $T(R)$ . Then the hydrostatic equilibrium equation becomes

$$\frac{1}{\rho} \frac{dP}{dz} = c^2 \frac{d \ln \rho}{dz} = - \frac{GMz}{(R^2 + z^2)^{3/2}}, \quad (8)$$

where  $c$  is the sound speed,  $P$  is the gas pressure,  $\rho$  is the gas density, and  $M$  is the central mass. This equation can be vertically integrated from the midplane to yield the gas density at height  $z$  above the surface in terms of the midplane gas density:

$$P = \rho c^2 = \rho_0 c^2 \exp \left\{ \frac{GM}{c^2} \left[ \frac{1}{(R^2 + z^2)^{1/2}} - \frac{1}{R} \right] \right\}. \quad (9)$$

In the limit  $z \ll R$ , the density distribution reduces to a Gaussian form (Shakura and Sunyaev 1973):

$$\rho \sim \rho_0 \exp \left[ \frac{GM}{Rc^2} \left( - \frac{1}{2} \frac{z^2}{R^2} \right) \right].$$

The total surface density is then approximately  $(2\pi)^{1/2}\rho_0 H$ , where the local scale height is  $H = (R^3 c^2/GM)^{1/2}$ .

The assumption is usually made that  $P(\text{ext})$  is fully given by the pressure distribution of the circumstellar material that would be present if there were no wind, in this particular case by equation (9) (Elmegreen 1978). This is true if the material is in exact Keplerian rotation, so that the radial equation of motion for the disk material can be neglected. It is not obvious that this is strictly true if flows are present in the region just below the shock surface. However, in cases of interest the wind-disk interaction takes place many scale heights above the disk midplane, where the density falls off so rapidly that any change in pressure leads to only a small repositioning of the shock surface. For this reason our approximation that  $P(\text{ext})$  is given by equation (9) should not lead to serious error, especially since the temperature of the disk gas is uncertain (see § VI).

Barral and Cantó (1981) derived boundary conditions for the interaction of a wind with a circumstellar toroid. For many T Tauri stars it is more likely that the disk extends all the way in to the star; otherwise, one would not be able to account for the observed near-infrared excess emission (Adams, Lada, and Shu 1987). In this case the solution depends upon the starting values of  $R$  and  $z$  (Elmegreen 1978). For these solutions we begin the integration arbitrarily at 1 AU, since essentially no emission of consequence comes from the inner regions where the disk is quite flat. We assume that the initial value of  $r'$  is given by

$$r'_0 = \frac{dr}{dH} \frac{dH}{d\theta} \sim \frac{4}{5} \frac{r^2}{H}. \quad (10)$$

The initial slope is the same as that for surfaces of constant scale height  $H$  if  $T \propto R^{-1/2}$  (so  $H \propto R^{5/4}$ ). This constraint can be inserted in equation (7a) to find the initial value of  $z$ . When integrating equation (7b), we further assume that  $W = 0$  initially. These boundary conditions are somewhat arbitrary, but solutions are initially reasonably smoothly varying. Furthermore, the solution at large distances is not sensitive to these assumptions (Elmegreen 1978). The reason once again is that the shock surface generally occurs at several scale heights above the midplane, so that the external pressure changes rapidly with position, and thus differing initial conditions yield little displacement in this surface.

From the solution of equations (7) we can find the wind density at the shock surface, the shock velocity  $v_s$ , and the wind velocity parallel to the surface,  $v_T$ . We make the assumption that the emitting gas has a velocity  $v_T$  only parallel to the shock surface, which is not unreasonable given the small shock velocities and the fact that the postshock velocity must be less than this.

The emission is then calculated by assuming that a series of plane-parallel shock models with appropriate parameters can be employed locally. We used a similar strategy to calculate the emission from bow shocks around Herbig-Haro objects (Hartmann and Raymond 1984; Hartigan, Raymond, and Hartmann 1987). The shock emission was computed by interpolation among the models given in Table 3.

The above assumptions for the velocity field of the emitting gas amount to assuming that the cooling distance is short, so that the flow follows the shock surface closely. For a typical shock velocity of  $30 \text{ km s}^{-1}$  and preshock density of  $10^5 \text{ cm}^{-3}$ , with preshock ionization of 1%, the gas takes 0.08 yr to cool down to  $1 \times 10^4 \text{ K}$  and 1.8 yr to cool to 5000 K (from an initial

postshock temperature of  $2.6 \times 10^4 \text{ K}$ ). The cooling distance perpendicular to the shock is not large, but the linear translations in the direction of motion at  $200 \text{ km s}^{-1}$  are 3.4 and 77 AU for cooling to  $1 \times 10^4$  and 5000 K, respectively. This suggests that the flow in region 2 (Fig. 4) will be relatively warm (several times  $10^3 \text{ K}$ ), and that adiabatic cooling could reduce the line fluxes by a significant factor, particularly for low values of  $\dot{M}$  and  $f$ . Turbulent mixing and/or additional shocking with disk material could help compress the flow and reduce cooling times. We neglect these complications in our profile calculations, but comment later on their effects.

## V. APPLICATIONS OF THEORY AND COMPARISON WITH OBSERVATIONS

### a) A Simple Model

Here we apply this theory to a simple disk model. We assume that the disk has a uniform surface density of  $12.5 \text{ g cm}^{-2}$  and a radial extent 100 AU (and therefore mass  $0.044 M_\odot$ ). We take a temperature distribution of  $T = 550 \text{ K} (r/1 \text{ AU})^{-1/2}$ , corresponding to simple radiative equilibrium for disk material around a star of effective temperature 4000 K and radius  $4 R_\odot$ . We assume a stellar mass of  $0.8 M_\odot$ . The wind is assumed to have an ionization fraction  $f = 0.01$  (see Appendix). We alternately use equations (7a) and (7b) to determine the shock surface.

The results for different mass-loss rates and terminal velocities are shown in Figures 5–7 and in Table 4. In general, the shape of the wind-disk shock surface is not very sensitive to the surface density  $\sigma$  or to  $\dot{M}$  or  $v_w$ . The reason is that the shock surface occurs about 4 scale heights above the midplane in this model, where the disk density varies very rapidly, so modest changes in ram pressure produce small changes in the height of

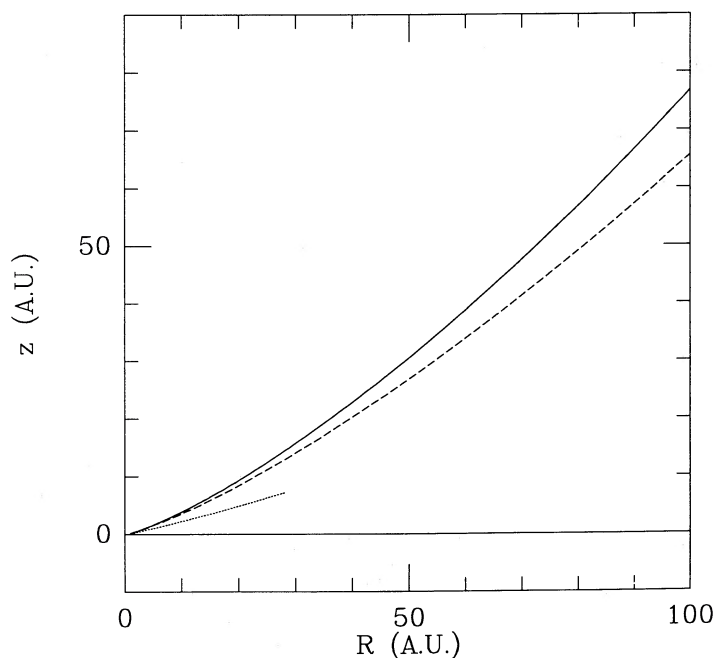


FIG. 5.—The location of the wind-disk shock for the models described in the text. The distances are given in units of AU. The solid line is the basic model (model 1 in Table 4), while the dashed line indicates the effect of the Cantó (1980) centrifugal correction (model 2). The dotted line is the  $z \propto r^{9/8}$  disk photosphere calculated by Kenyon and Hartmann (1987) to reproduce the infrared excess emission of typical T Tauri stars.

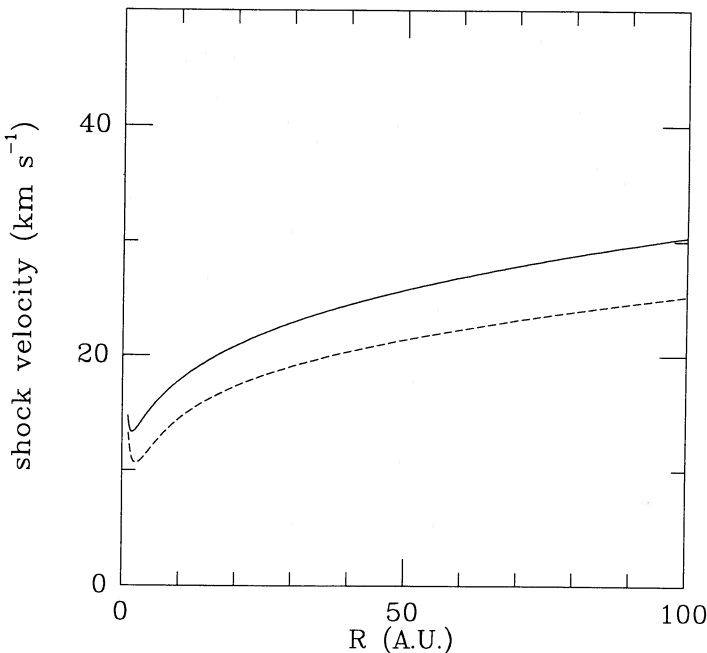


FIG. 6.—The shock velocity along the disk model surfaces shown in Fig. 5. The solid line is model 1, while the dashed line indicates the effect of the Cantó (1980) centrifugal correction (model 2). The jog at small radii is due to the approximate nature of the inner boundary conditions used (see text); the solution at large  $r$  is insensitive to the exact inner boundary conditions used.

the shock surface. For this same reason use of equation (7a) or (7b) makes only modest differences in the height of the wind-disk interface and in the line-profile shapes. The effect of the centrifugal term in equation (7b) is to flatten the shock surface and reduce its upward curvature. However, the resulting forbidden-line fluxes are sensitive to the shape of the shock surface and also to the assumed initial wind velocity, because the shocks are so oblique. Lower mass-loss rates also produce less emission; a model for  $\dot{M} = 10^{-8} M_{\odot} \text{ yr}^{-1}$  with the other parameters unchanged produces about 10 times less [O I] emission and about 5 times less [S II] emission.

The wind-disk shock models exhibit several encouraging features. Low-excitation emission is produced, in reasonable agreement with observed line ratios (Table 4). The [O I] and [S II] profiles calculated using equation (7a) (Fig. 7) are essentially indistinguishable, and the velocity widths and shifts show

that the amount of collimation produced by the flaring surface is in reasonable agreement with the values inferred observationally by Edwards *et al.* (1987). The line profiles computed using equation (7b) give similar results. We also note that two peaks in the line profiles are produced unless the system is observed very nearly pole-on (Fig. 7); such peaks are sometimes observed (AJO; Edwards *et al.* 1987; Fig. 1).

These calculations do not explicitly account for unshocked wind emission. As shown in Table 1, wind models with  $\dot{M} = 10^{-7} M_{\odot} \text{ yr}^{-1}$  and low X-ray ionization produce comparable [O I] fluxes without any disk interaction. The wind-velocity structure can be very different from that of the shocked gas, so the addition of the wind emission to the shock emission in Figure 7 could change the profiles considerably. Because the cooling wind contribution to [S II] is much smaller (Table 1), the combination of cooling wind and shocked wind could produce differences between the [S II] and [O I] profiles. In general, these lines seem to have fairly similar shapes (Edwards *et al.* 1987). The isotropic stellar wind assumed in our simple model does not have the collimation suggested by AJO and Edwards *et al.* (1987), and so the inner wind regions would produce much more redshifted [O I] emission than shown in Figure 7.

While the wind-disk shock model accounts for a number of qualitative features of the observations, there are problems with it as well. The principal difficulty is that the predicted luminosities of [O I] and [S II] are a factor of 3–10 times smaller than observed. It is hard to see how parameters in the simple model could be changed to increase the emission. Mass-loss rates in excess of  $10^{-7} M_{\odot} \text{ yr}^{-1}$  seem to be in severe conflict with stellar wind models (cf. DeCampli 1981; Hartmann, Edwards, and Avrett 1982). It is difficult to increase the line emission by increasing the stellar wind velocity, since this would also increase the observed average blueshifts of the emission lines. We could also extend the disk outward to somewhat larger radii, but given usual observing apertures this means extending our 100 AU disk out to perhaps 150–200 AU, resulting in possibly a factor of 2 or so increase in emission. We have also chosen a quite massive and “puffy” disk structure to maximize the shock-induced forbidden-line luminosity.

The use of equation (7a) assumes that the shocked wind flow is stopped without further energy loss by radiation in lines of interest. Thus, only  $\sim 2\%$  of the wind kinetic energy is thermalized to produce the calculated emission. Additional shocks in the flow could in principle increase the line emission fluxes significantly. We return to this point in § Vc.

TABLE 4  
FLUXES AND LINE RATIOS FOR WIND-DISK SHOCK MODEL

Model	[O I] <sup>a</sup>	[O II]/[O I]	[N II]/[O I]	[S II]/[O I]	$\lambda 6731/\lambda 6717$	[C I]/[O I]
1.....	1.5E+29	0.020	0.011	0.462	1.63	2.33
2.....	8.9E+28	0.019	0.008	0.618	1.41	2.94
3.....	2.5E+29	0.042	0.102	0.113	2.21	0.83
4.....	4.7E+29	0.027	0.080	0.088	2.25	0.77
5.....	5.2E+28	0.093	0.155	0.210	2.03	0.99

NOTES.—[O I] =  $\lambda 6300 + \lambda 6363$ , [O II] =  $\lambda 3727 + \lambda 3729$ , [N II] =  $\lambda 6583 + \lambda 6548$ , [S II] =  $\lambda 6717 + \lambda 6731$ , [C I] =  $\lambda 9650$ . Model 1:  $\dot{M} = 10^{-7} M_{\odot} \text{ yr}^{-1}$ ,  $v_w = 200 \text{ km s}^{-1}$ ,  $\sigma = 12.5 \text{ g cm}^{-2}$ ,  $r_{\text{max}} = 100 \text{ AU}$ , simple pressure balance (eq. [7a]). Model 2: same as model 1, except with centrifugal correction (eq. [7b]). Model 3: same as model 1, except with  $\dot{M} = 1 \times 10^{-7} M_{\odot} \text{ yr}^{-1}$  and  $v_w = 400 \text{ km s}^{-1}$ . Model 4: same as model 1, except with  $\dot{M} = 2 \times 10^{-7} M_{\odot} \text{ yr}^{-1}$  and  $v_w = 400 \text{ km s}^{-1}$ . Model 5: same as model 1, except with  $\dot{M} = 2 \times 10^{-8} M_{\odot} \text{ yr}^{-1}$  and  $v_w = 400 \text{ km s}^{-1}$ .

<sup>a</sup> Luminosity in units of  $\text{ergs s}^{-1}$ .

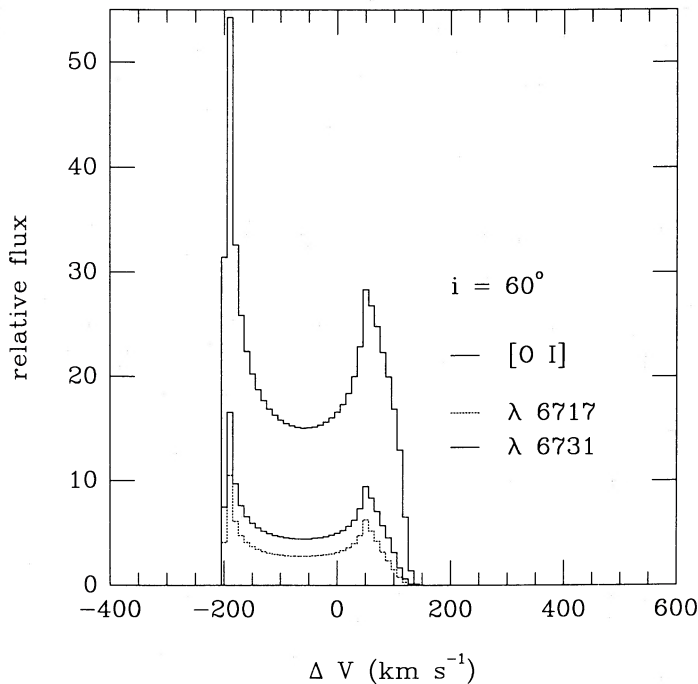


FIG. 7a

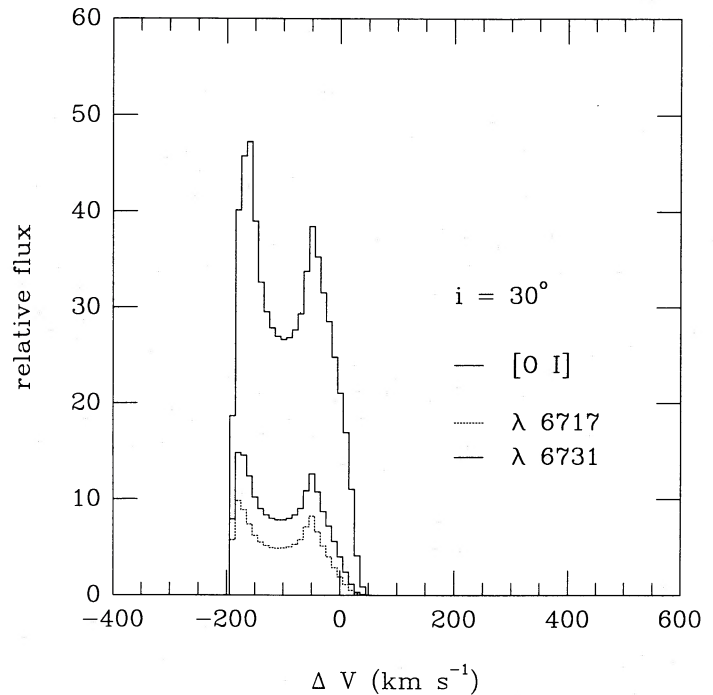


FIG. 7b

FIG. 7.—The forbidden-line emission profiles predicted by the wind-disk shock model of Figs. 6 and 7 (model 1). (a) Emission viewed from an angle of  $60^\circ$  from the disk axis. (b) Profiles seen at a viewing angle of  $30^\circ$  from the disk axis. (c) Profiles seen at a viewing angle of  $5^\circ$  from the disk axis.

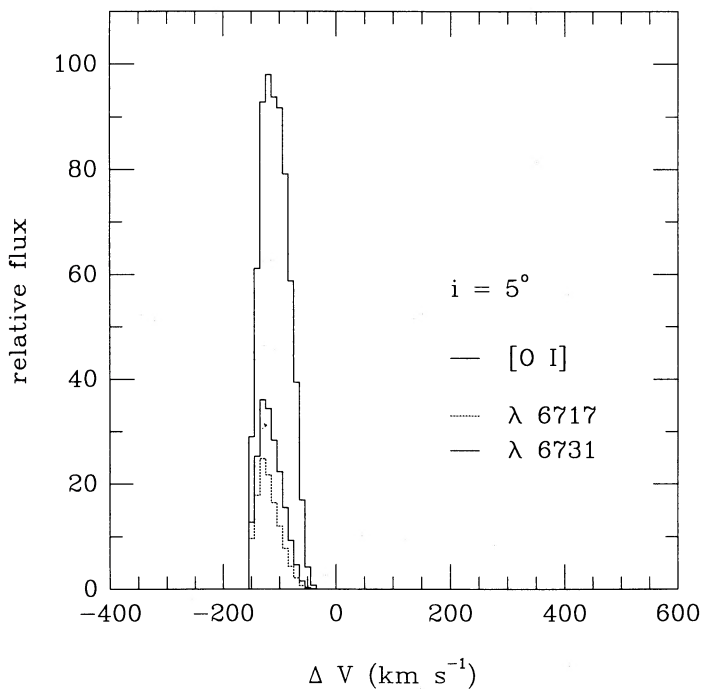


FIG. 7c

#### b) Disk Thickness

The disk thickness is a crucial parameter in our models, and merits further discussion. A dusty disk surrounding a T Tauri star will absorb light from the central object and reemit this energy in the infrared; the nature of the infrared spectrum places constraints on the temperature structure of the disk

(Adams and Shu 1986; Adams, Lada, and Shu 1987; Kenyon and Hartmann 1987, hereafter KH). Opaque dust disks whose thicknesses  $h$  scale as  $h \propto r^{9/8}$ , and whose surface temperatures consequently scale as  $T \propto r^{-0.6}$ , reproduce the average energy distributions of TTSs better than flat disk models (KH).

In Figure 5 we indicate this "average" disk "photosphere" inferred from matching the average T Tauri infrared excess spectrum. One can see that the wind-disk shock surface of our model is about twice as high in the vertical direction as the average disk photosphere. It is somewhat encouraging that there is observational evidence for disk thicknesses at least half what we need. On the other hand, the shock surface indicated in Figure 5 cannot be the disk photosphere for most T Tauri stars. Only a few objects exhibit the flat infrared spectra produced by such a thick disk (cf. Adams, Lada, and Shu 1987, 1988; KH). Such an opaque disk would obscure half of the sky as seen from the star, implying that half of all TTSs should be so obscured as to be detectable only at infrared wavelengths. *IRAS* surveys have turned up some embedded sources, but not nearly enough (Myers *et al.* 1987; Beichman *et al.* 1986). Thus the wind-disk interface of the model in Figure 5 cannot be the photospheric surface of the disk. Conversely, a shock surface given by the dotted line in Figure 5 would produce imperceptible [O I] and [S II] emission.

One possible resolution of this problem is that some dust settles out of the upper disk regions toward midplane (Weidenschilling 1980, 1984). This is especially plausible since the wind-disk interaction surface typically occurs several scale heights above the midplane. For example, in the model discussed above, at  $R = 72$  AU the shock surface is at  $z = 49.6$  AU, 4.2 local scale heights above the midplane. Thus the wind shocks in the tenuous outer atmosphere of the disk. Indeed, there may be difficulties in getting dust mixed as much as 2–3 scale heights above the midplane, as required by KH.

In a realistic model for the vertical temperature distribution where the central star provides all of the heating, one would expect the upper surfaces to be hotter than the disk midplane. Thus the optically thin upper scale heights of the disk might have temperatures falling off as  $r^{-1/2}$ , while the dense, cooler, optically thick regions would have lower temperatures. A detailed model is difficult to construct without a better understanding of grain opacities and dust diffusion.

### c) Flow Instabilities

The basic considerations sketched in § IIIb indicated that the disk does not have to be especially thick to produce the required emission as long as the disk surface is adequately tilted to the wind direction. The interface between shocked wind and disk material in our model may be subject to shock and Kelvin-Helmholtz instabilities (Elmegreen 1978). Since the shocks are so oblique, any slight perturbation which tilts the surface normal toward the star will result in a much larger ram pressure by the wind, driving the shock deeper into the disk and tilting the surface still more. Thus, instabilities may produce shocks that are less oblique, and hence have higher shock velocities, than predicted by the equilibrium model. Higher shock velocities mean larger emission luminosities, allowing flatter equilibrium disk surfaces to produce adequate fluxes.

Cassen (1987) has suggested to us that instabilities at the disk surface might create shock "wakes" that extend a significant distance above the disk surface, creating the required wind-shock heating with a relatively thinner disk. This effect may not be very important, given the relatively short cooling distances found perpendicular to the shock (although the cooling distances *along* the flow can be quite large; see § IV). Hydrodynamic calculations of the wind-shock interaction are desirable.

The instability-driven shocks might result in shock velocities that are too high, producing too much high-excitation emission like [N II]. We think that this will not occur, and the shocks will remain fairly oblique, because of the large density stratification inherent in the disk structure. Time-dependent calculations of the stability of oblique shocks with realistic cooling are needed to test our suggestion.

In the Cantó (1980) formulation, the postshock flow is assumed not to shock further, even though it must be curved around appreciably by the outer disk. Cantó cites arguments by Kahn (1980) that Kelvin-Helmholtz instabilities will not introduce substantial mixing. However, as noted by Elmegreen (1978), the situation is not exactly that of the usual Kelvin-Helmholtz instability, where flow is exactly parallel to the density stratification; the upward curvature of the disk ensures that the postshock flow has a different velocity vector than contours of constant pressure (see Fig. 4). Hence we expect that the wind may well be shocked a few times before leaving the system.

We note that  $20 \text{ km s}^{-1}$  shocks dissipate only about 1% of the total kinetic energy of a  $200 \text{ km s}^{-1}$  wind, and hence several shocks can occur without the wind losing an appreciable amount of its energy. If the wind is shocked several times, the mass-loss rate required to match the observed forbidden-line luminosity is correspondingly reduced.

We also note that some emission could result from instabilities driving shocks into disk material. We cannot predict the magnitude of this emission without a time-dependent calculation, but we speculate that some of the strong low-velocity

emission seen in TTSs might originate in such shocked disk material.

In summary, we suggest that wind-disk surface instabilities are likely to increase the shock-induced emission considerably over that produced by an equilibrium model. Such effects will work in the direction of producing better agreement with observations.

### d) Observational Predictions

The wind-disk shock model for the forbidden-line radiation makes several observational predictions. Higher wind velocities should generally produce larger shock velocities and thus higher excitation spectra. It is interesting that HL Tau, the only object in the Edwards *et al.* (1987) sample with fairly strong [N II], has a wind velocity of at least  $400 \text{ km s}^{-1}$ , a factor of 1.5–2 times larger than the velocity widths observed for the other stars. Scaling our basic model to a higher wind velocity, one finds shock velocities of  $40\text{--}50 \text{ km s}^{-1}$ , in the range needed to produce [N II] (if densities are low enough; Tables 3 and 4).

As discussed in § III, it is difficult to heat the wind at large distances by stellar energy fluxes. On the other hand, it is difficult to make the disk sufficiently thick close to the star without assuming unreasonably large temperatures. Therefore, direct spatial resolution of emitting regions of  $50\text{--}100 \text{ AU}$  in extent will strongly support the wind-disk shock interaction model. A radius of  $50 \text{ AU}$  at  $160 \text{ pc}$  corresponds to an angular diameter of  $\frac{2}{3}''$ , which can in principle be observed from the ground in good seeing or through speckle interferometry, and can be detected with the Hubble Space Telescope. (The electron densities estimated by Edwards *et al.* 1987 also imply such large emitting volumes. However, these calculations assume that the wind is fully ionized; if the hydrogen in the flow is mostly neutral, then the emitting volumes become smaller.)

To investigate the observability of extended forbidden-line emission, we have computed the surface brightness expected in [O I] for our model 1 looking down directly along the disk rotational axis. Because the shock velocities do not vary rapidly beyond about  $10 \text{ AU}$ , one would expect the surface brightness to vary roughly as  $r^{-2}$ , the variation of the preshock density; and detailed calculations verify this (Fig. 8). The rapid falloff of surface brightness with distance may make observation difficult. However, if the disk axis is tilted to some degree, limb brightening should occur, and produce an enhanced forbidden-line surface brightness along a direction perpendicular to the disk axis.

If spectra with sufficient spatial resolution can be obtained, one can look for the characteristic position-velocity profile of the model. Viewed pole-on, the wind-disk shock model predicts that the most negative radial velocity material will be seen at the periphery of the forbidden-line emission. The latitude-dependent wind model of Edwards *et al.* (1987) predicts the reverse.

As shown in the previous section, the disk-wind mechanism requires an extended, optically thin upper disk envelope. Thus the connection between the shock surface and the disk photosphere, where light from the central star is reprocessed, is indirect. Nevertheless, one expects that stars with larger infrared excesses due to reprocessing should generally have thicker disk envelopes and thus more wind-disk shock emission. There does seem to be some evidence for such a correlation. In the survey of Taurus-Auriga by Strom *et al.* (1988), 15 of the 18 stars with infrared luminosities  $\geq 0.5$  times the stellar luminosity have

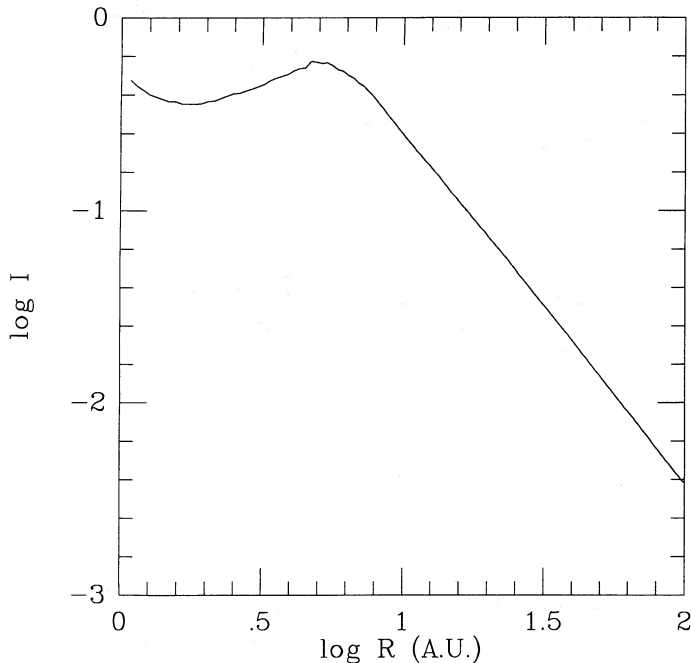


FIG. 8.—Surface brightness of [O I] calculated for model 1, observed looking down along the disk axis

[O I] equivalent widths  $\geq 1 \text{ \AA}$ ; conversely, only five of the 38 stars with  $L_{\text{IR}} \leq 0.5 L_{\star}$  have such [O I] emission. Of course, broad [O I] emission in a star without IR excess, and hence without a circumstellar disk (Adams, Lada, and Shu 1987; KH), would be hard to explain with a wind-disk shock.

The model predicts that some TTSs might be viewed through a relatively dust-free gaseous envelope of density  $\sim 10^7 \text{ cm}^{-3}$  and column densities  $\sim 10^{22}\text{--}10^{23} \text{ cm}^{-2}$ . Thus one might find excess “interstellar” absorption in lines like Ca II, Mg II, Na I, without the consequent dust absorption (since the dust has presumably settled closer to the midplane).

Another model prediction is the strong [C I] emission shown in Table 4. The [C I] strength is the most sensitive of all the predictions to the assumption of a small cooling length and to the electron density in the shocked gas. It is also likely that photoionization of C I from the  $^1D$  level by stellar Ly $\alpha$  will drastically reduce the neutral carbon population. Therefore, while a search for [C I] emission would be interesting, we do not consider it a test of the model. [C I] emission will also be reduced if molecular cooling in the postshock region is important.

Torrelles *et al.* (1985) and Rodríguez *et al.* (1986) have suggested, in a similar context, that thermalization of  $\sim 5\%$  of a stellar wind with  $\dot{M} = 10^{-7} M_{\odot} \text{ yr}^{-1}$  and  $v_w = 400 \text{ km s}^{-1}$  could produce observable radio continuum emission. Our models produce far too little thermal emission to be observable. Instabilities or disk irregularities might enhance the emission considerably. It is not obvious that the radio emission observed from TTSs (Bieging, Cohen, and Schwartz 1984) is produced by this mechanism; there is no clear correlation between forbidden-line flows and radio emission.

Finally, we suggest that if the shocked wind-disk interface is unstable, shocks may be driven into disk material which produce observable emission. The emission lines produced should be relatively narrow and near the stellar rest velocity because of the low velocity of disk material. Emission from the disk might be especially important for low- $\dot{M}$  flows, where the cooling times for the shocked wind are very long, preventing or reducing shocked wind emission.

#### e) Implications for T Tauri Winds

Edwards *et al.* (1987) concluded that models in which the winds of TTSs are latitude-dependent, with maximum velocity along the disk axis, are in best agreement with the observations. We could incorporate such a stellar wind into our disk-wind model with little difficulty, but we have not because the model already involves many parameters.

One of the advantages of a latitude-dependent wind is that it produces peaks of different height in the emission profiles (Edwards *et al.* 1987), whereas our simple axisymmetric model predicts essentially equal peaks (Fig. 7). However, the observed inequality of [O I] peaks in a few objects (notably DO, Tau, DF Tau, HL Tau; Fig. 1 of Edwards *et al.*) is not matched either by the models of Edwards *et al.* (1987). We think that such large profile asymmetries indicate strong departures from axisymmetry, which are not easy to incorporate in other than an ad hoc manner.

One of the implications of our model is that some T Tauri stars eject a lot of mass near the equatorial plane, the exact opposite of a “jet” model. This does not rule out the presence of jets, but it does emphasize the importance of near-equatorial flow. It is likely that the near-equatorial flow is more efficient in removing angular momentum than a jet along the rotation axis. Since T Tauri stars are generally slow rotators (Bouvier *et al.* 1986), the ejection traced by [O I] emission may play an important role in early stellar evolution.

#### VI. SUMMARY

We may find that many features of the forbidden-line emission in T Tauri stars can be explained by a model where the stellar wind shocks obliquely with a relatively massive circumstellar disk. The model requires substantial equatorial mass loss from the T Tauri star, and a somewhat thick disk. The disk can be sufficiently thick if its outer few scale heights are relatively dust-free, with a temperature falling off with distance roughly as  $r^{-1/2}$ . Alternatively, instabilities in the wind-disk interface might produce sufficient emission with flatter disks. In any event, such instabilities are likely to control the forbidden-line luminosity. High spatial resolution observations can provide further tests of the model.

John Stauffer took and reduced a large number of the 4 m echelle spectra. We also wish to thank Darryl Willmarth for assistance with the 4 m echelle observations. We acknowledge useful conversations with Suzan Edwards, Pat Cassen, and Pat Hartigan, and a helpful referee’s report from Jorge Cantó. This research was supported by National Aeronautics and Space Administration grants NAGW 511 and NAGW 528.

## APPENDIX

## T TAURI WIND IONIZATION

Here we justify our choice of  $f = 0.01$  for the preshock ionization state in our wind-disk shock models. If we assume spherical flow with no significant source of ionizing radiation or other heating, and assume that the electron density equals the proton density, the ionization state of hydrogen varies as

$$\frac{\alpha N_0 r_0^2}{v} \left( \frac{1}{r} - \frac{1}{r_0} \right) = \frac{1}{f_0} - \frac{1}{f},$$

where  $f_0$  and  $r_0$  are the values of the ionization fraction and radius at the inner boundary and  $\alpha$  is the recombination rate coefficient. In this equation we have neglected the temperature dependence of  $\alpha$ . In the limit of interest, where  $r \gg r_0$  and  $f \ll f_0$ , we find

$$f = 0.02 \frac{v_{7.3}^2 r_{11.5}}{\alpha_{-12.5} \dot{M}_{-8}}.$$

Here  $\alpha_{-12.5}$  is the recombination rate coefficient in units of  $3 \times 10^{-13} \text{ cm}^3 \text{ s}^{-1}$  (recombination to  $n \geq 2$  at  $10^4 \text{ K}$ ),  $\dot{M}_{-8}$  is the mass-loss rate in units of  $10^{-8} M_\odot \text{ yr}^{-1}$ ,  $v_{7.3}$  is the wind velocity in units of  $200 \text{ km s}^{-1}$ , and  $r_{11.5}$  is the initial radial distance in units of  $3 \times 10^{11} \text{ cm}$ ,  $\sim R_*$  for T Tauri stars.

Calvet and Hartmann (1988) find that wind temperatures for T Tauri stars must fall below  $10^4 \text{ K}$  inside of a few stellar radii for mass-loss rates  $\geq 10^{-8} M_\odot \text{ yr}^{-1}$  in order to avoid excessive Mg II fluxes. If no wind ionization thus occurs beyond  $r_0 = 5 R_*$ , this constraint implies  $f \lesssim 10\%$ . For larger mass-loss rates, the Mg II flux constraint implies even smaller  $r_0$ , and thus considerably smaller values of  $f$ . As a lower limit, it seems likely that carbon, iron, and silicon will be singly ionized under expected conditions, especially with a large stellar Ly $\alpha$  ionizing flux, so we expect  $f \gtrsim 0.1\%$ . Thus  $f = 0.01$  seems to be a reasonable intermediate guess.

## REFERENCES

- Adams, F. C., and Shu, F. H. 1986, *Ap. J.*, **308**, 836.  
 Adams, F. C., Lada, C. J., and Shu, F. H. 1987, *Ap. J.*, **312**, 788.  
 ———. 1988, *Ap. J.*, **326**, 865.  
 Allen, C. W. 1973, *Astrophysical Quantities* (3d ed.; London: Clowes).  
 Appenzeller, I., Jankovics, I., and Ostreicher, R. 1984, *Astr. Ap.*, **141**, 108 (AJO).  
 Barral, J. F., and Cantó J. 1981, *Rev. Mexicana Astr. Ap.*, **5**, 101.  
 Beichman, C. A., Myers, P. C., Emerson, J. P., Harris, S., Mathieu, R., Benson, P. J., and Jennings, R. E. 1986, *Ap. J.*, **307**, 337.  
 Belcher, J. W., and MacGregor, K. B. 1976, *Ap. J.*, **210**, 498.  
 Biegging, J. H., Cohen, M., and Schwartz, P. R. 1984, *Ap. J.*, **282**, 699.  
 Bouvier, J., Bertout, C., Benz, W., and Mayor, M. 1986, *Astr. Ap.*, **165**, 110.  
 Brown, A., Ferraz, M. C. de M., and Jordan, C. 1984, *M.N.R.A.S.*, **207**, 831.  
 Butler, S. E., and Dalgarno, A. 1980, *Ap. J.*, **241**, 838.  
 Calvet, N., and Hartmann, L. 1988, in preparation.  
 Cantó, J. 1980, *Astr. Ap.*, **86**, 327.  
 Cantó, J., Tenorio-Tagle, G., and Rozyczka, M. 1988, *Astr. Ap.*, **192**, 287.  
 Cassen, P. 1987, private communication.  
 Chernoff, D. F., Hollenbach, D. J., and McKee, C. F. 1982, *Ap. J. (Letters)*, **259**, L97.  
 Cox, D. P., and Raymond, J. C. 1985, *Ap. J.*, **298**, 651.  
 Cram, L. E., Giampapa, M. S., and Imhoff, C. L. 1980, *Ap. J.*, **238**, 905.  
 DeCampi, W. M. 1981, *Ap. J.*, **244**, 124.  
 Draine, B. T., Roberge, W. G., and Dalgarno, A. 1983, *Ap. J.*, **264**, 485.  
 Edwards, S. 1988, private communication.  
 Edwards, S., Cabrit, S., Strom, S. E., Heyer, I., and Strom, K. M. 1987, *Ap. J.*, **321**, 473.  
 Elmegreen, B. G. 1978, *Moon and Planets*, **19**, 261.  
 Hartigan, P., Raymond, J. C., and Hartmann, L. 1987, *Ap. J.*, **316**, 323.  
 Hartmann, L. 1986, *Fund. Cosmic Phys.*, **11**, 279.  
 Hartmann, L., Edwards, S., and Avrett, E. 1982, *Ap. J.*, **261**, 279.  
 Hartmann, L., Hewett, R., Stahler, S., and Mathieu, R. D. 1986, *Ap. J.*, **309**, 275.  
 Hartmann, L., and Raymond, J. C. 1984, *Ap. J.*, **276**, 560.  
 Hayes, W. D., and Probst, R. F. 1966, *Hypersonic Flow Theory* (2d ed.; New York: Academic), p. 129.  
 Jankovics, I., Appenzeller, I., and Krautter, J. 1982, *Pub. A.S.P.*, **95**, 883 (JAK).  
 Kahn, F. D. 1980, *Astr. Ap.*, **83**, 303.  
 Kenyon, S. J., and Hartmann, L. 1987, *Ap. J.*, **323**, 714 (KH).  
 Königl, A. 1982, *Ap. J.*, **261**, 115.  
 Kuan, P. 1975, *Ap. J.*, **202**, 425.  
 Kuhl, L. V. 1964, *Ap. J.*, **140**, 1409.  
 Lago, M. T. V. T., Penston, M. V., and Johnstone, R. M. 1985, *M.N.R.A.S.*, **212**, 151.  
 Mauche, C. W., and Raymond, J. C. 1987, *Ap. J.*, **323**, 690.  
 Mundt, R. 1985, in *Protostars and Planets II*, ed. D. C. Black and M. S. Matthews (Tucson: University of Arizona Press), p. 414.  
 Myers, P. C., Fuller, G. A., Mathieu, R. D., Beichman, C. A., Benson, P. J., Schild, R. E., and Emerson, J. P. 1987, *Ap. J.*, **319**, 340.  
 Natta, A., Giovanardi, C., and Palla, F. 1988, *Ap. J.*, **332**, 921.  
 Neufeld, D. A. 1987, Ph.D. thesis, Harvard University.  
 Nussbaumer, H., and Storey, P. J. 1983, *Astr. Ap.*, **126**, 75.  
 Pudritz, R. E., and Norman, C. A. 1983, *Ap. J.*, **274**, 677.  
 Rawlings, J. M. C., Williams, D. A., and Cantó, J. 1988, *M.N.R.A.S.*, **230**, 695.  
 Rodriguez, L. F., Cantó, J., Torrelles, J. M., and Ho, P. T. P. 1986, *Ap. J. (Letters)*, **301**, L25.  
 Schwartz, R. E. 1983, *Ann. Rev. Astr. Ap.*, **21**, 209.  
 Shakura, N. I., and Sunyaev, R. A. 1973, *Astr. Ap.*, **24**, 337 (SS).  
 Strom, S. E., Strom, K. M., Kenyon, S. J., and Hartmann, L. 1988, *A.J.*, **95**, 534.  
 Torrelles, J. M., Ho, P. T. P., Rodriguez, L. F., and Cantó, J. 1985, *Ap. J.*, **288**, 595.  
 Weidenschilling, S. J. 1980, *Icarus*, **44**, 172.  
 ———. 1984, *Icarus*, **60**, 553.

LEE HARTMANN and JOHN RAYMOND: Center for Astrophysics, 60 Garden Street, Cambridge, MA 02138